https://doi.org/10.5194/amt-2020-173
Preprint. Discussion started: 23 June 2020

Atmospheric Measurement Techniques Discussions

Diurnal variability of total column NO_2 measured using direct solar and lunar spectra over Table Mountain, California (34.38°N)

King-Fai Li[1], Ryan Khoury[1], Thomas J. Pongetti[2], Stanley P. Sander[2], Yuk L. Yung[2,3]

[1]Department of Environmental Science, University of California, Riverside, California, USA
[2]Jet Propulsion Laboratory, California Institute of Technology, Pasadena, California, USA
[3]Division of Geological and Planetary Sciences, California Institute of Technology, Pasadena, California, USA

Correspondence to: King-Fai Li (king-fai.li@ucr.edu)

Abstract. A full diurnal measurement of total column NO_2 has been made over the Jet Propulsion Laboratory's Table Mountain Facility (TMF) located in the mountains above Los Angeles, California, USA (2.286 km above mean sea level, 34.38°N, 117.68°W). During a representative week in October 2018, a grating spectrometer measured the telluric NO_2 absorptions in direct solar and lunar spectra. The total column NO_2 is retrieved using a model-based minimum-amount Langley extrapolation, which enables us to accurately treat the non-constant NO_2 diurnal cycle abundance and the effects of pollution near the measurement site. The measured 24-hour cycle of total column NO_2 on clean days agrees with a 1-D photochemical model calculation, including the monotonic changes during daytime and nighttime due to the exchange with the N_2O_5 reservoir and the abrupt changes at sunrise and sunset due to the activation or deactivation of the NO_2 photodissociation. The observed daytime NO_2 increasing rate is $(1.29 \pm 0.30) \times 10^{14}$ cm^{-2} h^{-1}. The total column NO_2 in one of the afternoons during the measurement period was much higher than the model simulation, implying the influence of urban pollution from nearby cities. A 24-hour back-trajectory analysis shows that the wind first came from inland in the northeast and reached the southern Los Angeles before it turned northeast and finally arrived TMF, allowing it to pick up pollutants from Riverside County, Orange County, and Downtown Los Angeles.

1 Introduction

Nitrogen dioxide (NO_2) plays a dominant role in the ozone (O_3)-destroying catalytic cycle (Crutzen, 1970). NO_2 column abundance has been measured using ground-based instruments since the mid-1970s (Network for the Detection of Atmospheric Composition Change, http://www.ndacc.org), which serve as the standards for validating satellite measurements. Noxon (1975) and Noxon et al. (1979) retrieved the stratospheric NO_2 column by differential optical absorption spectroscopy (DOAS) in the visible spectral range using ratios of scattered sunlight from the sky and direct sun/moonlight at low (noon/midnight) and high (twilight) air mass factors over Fritz Peak, Colorado (39.9°N). Since the optical path of sun/moonlight at dawn or dusk (solar/lunar zenith angle ≈ 90°) is much longer than the optical path of the direct sunlight at noon/midnight, the NO_2 absorption in the noon/midnight spectrum can be assumed to be small and the NO_2 absorption in the twilight slant column could therefore be isolated effectively by ratioing the scattered twilight spectrum to the scattered noon

https://doi.org/10.5194/amt-2020-173
Preprint. Discussion started: 23 June 2020


Atmospheric Measurement Techniques Discussions

spectrum. This DOAS principle also applies to ratios of direct moonlight or sunlight at low and high air mass factors. Noxon et al.'s (1979) measurements revealed sharp changes of the stratospheric NO_2 column before and after sunsets and sunrises at mid-latitudes. Similar DOAS measurements at high latitudes in the 1980s focused on the role of NO_x in controlling O_3 and active halogen species in the polar stratosphere (Fiedler et al., 1993; Flaud et al., 1988; Keys and Johnston, 1986; Solomon, 1999). Johnston and McKenzie (1989) and Johnston et al. (1992) reported a reduction in the southern hemispheric NO_2 over Lauder, New Zealand (45.0°S), following the eruptions of El Chichón (in 1982) and Pinatubo (in 1991), respectively.

NO_2 column abundance has also been measured using direct solar spectra acquired by Fourier-Transform infrared (FTIR) spectrometers. Advantages of direct solar measurements are the lack of Raman scattering in the spectra, air mass factors determined geometrically rather than through a radiative transfer code, and provision of NO_2 column abundances at most times during the day. Sussmann et al. (2005) retrieved the stratospheric NO_2 column abundance over Zugspitze, Germany (47°N) using the infrared absorption in the solar spectrum near 3.43 μm. The stratospheric NO_2 column abundance was then subtracted from the total column estimated from satellite measurements to obtain the tropospheric column. Wang et al. (2010) demonstrated how high spectral resolution measurements using a Fourier transform spectrometer could perform absolute NO_2 column abundance retrievals without the need for a solar reference spectrum. Because of the solar rotation, the Fraunhofer features in the UV spectra acquired simultaneously from the east and west limbs of the solar disk are Doppler shifted while the telluric NO_2 absorptions are not shifted (Iwagami et al., 1995). Thus, the telluric NO_2 absorptions can be identified by correcting the Doppler shift without the need of an *a priori* solar spectrum. Other techniques, such as balloon-based *in situ* measurements (May and Webster, 1990; Moreau et al., 2005), balloon-based solar occultations (Camy-Peyret, 1995) and ground-based multi-axis DOAS (MAX-DOAS; Hönninger et al., 2004; Sanders et al., 1993), have also been employed to further characterize the vertical distributions of NO_2.

Here we retrieve the total column NO_2 over Table Mountain Facility (TMF) in Wrightwood, California, USA (2.286 km above mean sea level, 34.38°N, 117.68°W) using Langley extrapolation to determine the reference spectrum and considering both daytime and night time chemistry. Daytime NO_2 concentration remains significant, albeit small relative to the night-time concentration, and varies from morning to afternoon. This daytime variation has traditionally been a source of error in determination of the DOAS reference spectrum using Langley extrapolation. Comprehensive assessment of NO_2 must include both daytime and nighttime values. We therefore also retrieve daytime column NO_2 by acquiring direct sun spectra throughout the day. We will compare the daytime and nighttime total column NO_2 with those simulated in a one-dimensional (1-D) photochemical model. The effect of urban pollution on the measured total column NO_2 can be deduced from this comparison.

https://doi.org/10.5194/amt-2020-173
Preprint. Discussion started: 23 June 2020


Atmospheric Measurement Techniques Discussions

2 Data and Method

2.1 Instrumentation and measurement technique

The grating spectrometer used for the NO_2 spectral measurement is similar to the one used by Chen et al. (2011) and is installed in the same observatory. A heliostat and a telescope are used to direct and launch light into a fibre optic bundle placed at the focal plane of the telescope (Figure 1). The bundle consists of 19 silica fibres, 200 μm in diameter, arranged in a circular configuration (in SMA 905 connectors) on the source end and in a linear pattern on the spectrograph end. Before entering the spectrograph, light is passed through an order sorting filter (Schott GG-400 glass) and a shutter. The imaging spectrograph is a Princeton Instruments SP-2-300i with a 0.3-m focal length used with a 1200 g mm^{-1} grating blazed at 500 nm. A CCD detector (Princeton Instruments PIXIS 400B) is placed at the focal plane of the spectrograph. The 1340 × 400 imaging array of 20 × 20 μm^2 pixels are vacuum sealed and thermoelectrically cooled to −80 °C.

We acquired direct moon and direct sun spectra for lunar/solar zenith angles less than 80° and 5 to 7 days surrounding the full moon. When direct sunlight was used, two ground glass diffuser plates were inserted into the beam prior to the telescope primary to integrate over the entire solar disk and to attenuate light. Additional attenuation of light to avoid detector saturation was accomplished by placing a 23% open area screen in the beam just after the diffuser plates. The resulting spectrum has a spectral grid spacing on the detector of 0.048 nm from 411 nm to 475 nm with a measured line shape of 0.34-nm FWHM sampled at ~7 pixels. Spectral calibration and line shape measurements were accomplished using a diffuse reflection of an Argon lamp near the fibre end, which gives a nearly linear result between pixel and wavelength with a small second order correction; the second order correction is considered in the calibration and the fitting. The exposure time was 4 s and 0.25 s during the lunar/solar noon observations, respectively. At higher zenith angles, longer exposures were taken to keep the detector counts in the same range. The data were dark corrected and averaged to obtain the desired signal levels; for the sun, this was consistently ~4 minutes; for the moon, the averaging time varied from ~8 minutes during the night of the full moon to 24 minutes on the night 3 days from full moon.

2.2 The DOAS retrieval

The DOAS technique is used to retrieve the NO_2 slant column (Noxon, 1975; Noxon et al., 1979; Platt et al., 1979; Stutz and Platt, 1996). A spectrum measured by the grating spectrometer at any time of the day is ratioed to a pre-selected reference spectrum. From the ratioed spectrum, we retrieve the differential slant column NO_2 relative to the column that is represented by the reference spectrum. The total slant column is then the sum of the differential slant column and the reference column.

Our reference spectrum is a solar spectrum measured at the TMF ground level at local noon (Chen et al., 2011). This solar reference spectrum is used to ratio all other spectra collected, including those during the solar and lunar measurement cycles. In principle, one can retrieve the reference NO_2 column from the reference spectrum. However, this requires precise knowledge of the solar spectrum at the top of the atmosphere in order to isolate the NO_2 absorption. We will use a variant of

https://doi.org/10.5194/amt-2020-173
Preprint. Discussion started: 23 June 2020

Atmospheric Measurement Techniques Discussions

the Langley extrapolation to circumvent the need of the retrieval of the reference column (Lee et al., 1994; Herman et al., 2009); see following section for details.

The differential slant column NO_2 is retrieved by fitting the ratioed spectrum between 430 and 468 nm. The spectral fitting is accomplished through the Marquardt-Levenberg minimization using QDOAS retrieval software (http://uv-vis.aeronomie.be/software/QDOAS/). The highly spectrally resolved NO_2 absorption cross sections at $T = 215\ \mathrm{K}, 229\ \mathrm{K}, 249\ \mathrm{K}, 273\ \mathrm{K}, 298\ \mathrm{K}$, and $299\ \mathrm{K}$ based on Nizkorodov et al. (2004) are convolved to the instrument resolution using the instrument line shape function and the Voigt line shape prior to its use in QDOAS. The temperature profile for the calculation of the Voigt line shape is determined by the yearly average of the TMF temperature lidar measurements. In addition to NO_2, other absorptions by O_3, O_4 (O_2 dimer), and H_2O in the same spectral window are simultaneously retrieved. The NO_2 abundance retrieved from QDOAS is the desired differential slant column NO_2 relative to our chosen reference spectrum.

2.3 The model-based minimum-amount Langley extrapolation

Let y be the differential slant column NO_2 along the line-of-sight, y_0 the reference column NO_2, m the stratospheric airmass factor (which is proportional to the geometric secant of the solar zenith angle in the stratosphere for these direct solar and lunar observations), and x the total vertical column NO_2; x is our target quantity. The differential slant column can be approximated as the total vertical column multiplied by the stratospheric airmass factor after the subtraction of the reference column:

$$y = m\,x - y_0 \tag{1}$$

If y_0 were known, then x would be simply $m^{-1}(y + y_0)$. The Langley extrapolation technique for determination of the extra-terrestrial reference obtains x and $-y_0$ as the slope and the intercept of the linear regression of y against m, respectively, assuming x is temporally constant (i.e. the vertical column does not change during the course of the day). In this formulism, the reference column y_0 is an extrapolated value corresponding to hypothetical zero airmass ($m = 0$).

The Langley extrapolation was first used to measure the solar spectrum at the top of the atmosphere (Langley, 1903) and has also been used to measure atmospheric constituents (e.g., Jeong et al., 2018; Toledano et al., 2018; Barreto et al., 2017; Huber et al., 1995; Bhartia et al., 1995). However, the assumption of a constant x is often violated due to diurnal variabilities in the atmospheric constituents driven by, *e.g.*, the incident solar radiation, transmittance, circulation, and human activities. In our case, the afternoon total column NO_2 is greater than the morning total column NO_2 (see our Figure 3). Several modifications have been proposed to relax the assumption of a constant x (e.g., Ångström, 1970; Shaw, 1976; Long and Ackerman, 2000; Cachorro et al., 2008; Kreuter et al., 2013; Marenco, 2007). In this work, we combine the modifications used in Lee et al. (1994) and Herman et al. (2009) to account for the effects due to the NO_2 diurnal variability and urban pollution.

Lee et al. (1994) replaced the constant x with an *a priori* function of m, denoted by $x_a(m)$:

https://doi.org/10.5194/amt-2020-173
Preprint. Discussion started: 23 June 2020

Atmospheric Measurement Techniques Discussions

$$y = \alpha\, m\, x_a(m) - y_0, \tag{2}$$

Eq. (2) is analogous to Eq. (1) except that now y is regressed against the product $m\, x_a(m)$; α is the target quantity that will be obtained from the slope of the regression line. α serves as an effective scaling factor that adjusts the chemical rates in the model. Eq. (2) presents a model-based Langley extrapolation.

As in Lee et al. (1994), assuming the chemical processes of NO_2 are much faster than the dynamical processes so that the NO_2 diurnal cycle is at photochemical equilibrium, we obtain $x_a(m)$ from a 1-D photochemical model (to be described in the next section). The $x_a(m)$ we use corresponds to a clean atmosphere only. To perform the regression, we plot y against the product $m\, x_a(m)$ (Figure 2, blue open circles). If all NO_2 columns are measured on clean days, then they would ideally fall on a straight line. However, if there is a pollution source near a measurement site, then some of the measured NO_2 column may be significantly higher than $x_a(m)$, leading to a vertical spread in the scattered plot. The deviation from $x_a(m)$ may be highly variable, depending on the source types and the meteorology. When a large number of measured NO_2 columns on clean and polluted days are plotted together against $m\, x_a(m)$, the baseline of the scattered data may be considered as the NO_2 diurnal cycle in a clean atmosphere (Herman et al., 2009). Following Herman et al.'s (2009) terminology, we call our method the model-based minimim-amount Langley extrapolation.

To obtain the baseline, we divide the range of $m\, x_a(m)$ (from $\sim 5 \times 10^{15}$ to 3×10^{16} molecules cm^{-2} during our campaign) into 20 equal bins. Herman et al. (2009) used the 2-percentile of the y distribtion in each bin to define a baseline. To enhance the statistical robustness of the baseline, we use the 20-percentile instead (Figure 2, green dots). We fit the 20-percentile baseline to Eq. (2) and obtain the values of α and y_0 (Figure 2, red line). The fitted line in Figure 2 gives $\alpha = 0.88$ and $y_0 = 5.77 \times 10^{15}$ molecules cm^{-2}. This value of y_0 is our reference column used for both daytime and nighttime measurements.

2.4 The photochemical model

Our $x_a(m)$ is based on the Caltech/JPL 1-D photochemical model (Allen et al., 1984; Allen et al., 1981), shown as the black solid line in Figure 3. This photochemical model includes the stratospheric species that are important for O_3, odd-nitrogen (NO_x = N + NO + NO_2 + NO_3 + $2N_2O_5$) and odd-hydrogen (HO_x = H + OH + HO_2) chemistry, including the reactions discussed in Section 3.1. Nitrous oxide (N_2O) is the main parent molecule of NO_2 in the lower stratosphere. The concentration of N_2O at the ground level of the model is fixed at 330 ppb (https://www.esrl.noaa.gov/gmd/hats/combined/N2O.html). The kinetic rate constants are obtained from the 2015 JPL Evaluation (Burkholder et al., 2015).

The sunrise/sunset times and the solar noontime in the model are calculated using the ephemeris time. We use Newcomb parameterizations of the perturbations due to the Sun, Mercury, Venus, Mars, Jupiter, and Saturn (Newcomb, 1898). We also use Woolard parameterizations for the nutation angle and rate (Woolard, 1953). More modern calculation of the

https://doi.org/10.5194/amt-2020-173
Preprint. Discussion started: 23 June 2020


Atmospheric Measurement Techniques Discussions

ephemeris time may be used (e.g., Folkner et al., 2014) but the difference in the resulting ephemeris time is small (less than 0.1 s) and does not significantly impact our model simulation.

We progress the model in time until the diurnal cycle of the stratospheric NO_2 becomes stationary. Throughout the progression, the pressure and temperature profiles are fixed and do not vary with time. The model latitude is set at 34.38°N and the model day is set as October 26. The total column NO_2 is the vertical integral of the NO_2 concentration. The simulation represents the NO_2 abundance in a clean atmosphere without tropospheric sources.

3 Results and Discussions

3.1 Diurnal variation in total column NO_2

Figure 3 presents our preliminary observational data (colour dots) obtained during October 23–28, 2018. During the measurements, the skies were mostly clear or only partly cloudy, so we were able to make continuous solar spectral measurements throughout the whole period. During October, the local sunrise and sunset time were around 07:00 PST and 18:00 PST, respectively. At sunrise and sunset, the ambient twilight in the background of the moonlight occultation should be accounted for in the NO_2 retrieval, which is beyond the scope of this work. For this work, we exclude lunar total column NO_2 data when the ambient scattered twilight, including those from civil sources, is significant, which typically occurs when the lunar elevation angle is less than 6° above the horizon. The solid black line of Figure 3 is the simulated 24-hour cycle of the total column NO_2 variability in the 1-D model. The dashed line is a second simulation with a slightly lower temperature (see Section 3.3). Overall, the baseline simulation captures the observed trends during the daytime and the nighttime.

On most days, the total column NO_2 over TMF increased from $\sim 2 \times 10^{15}$ molecules cm^{-2} in the morning to $\sim 3.5 \times 10^{15}$ molecules cm^{-2} in the evening. There are 3 main sources of NO_x contributing to the daytime increase. The ultimate source is the reaction of N_2O with excited oxygen $O(^1D)$ resulting from the photolysis of O_3 in the stratosphere between 20–60 km, which produces nitric oxide (NO) molecules and eventually NO_2 through the NO_x cycle aided by O_3:

$$N_2O + O(^1D) \rightarrow NO + NO, \quad \text{(R1)}$$

$$NO + O_3 \rightarrow NO_2 + O_2. \quad \text{(R2)}$$

Another major source is the photolysis of the reservoir species, nitric acid (HNO_3) and dinitrogen pentoxide (N_2O_5):

$$HNO_3 + h\nu \rightarrow NO_2 + OH, \quad \text{(R3)}$$

$$N_2O_5 + h\nu \rightarrow NO_2 + NO_3. \quad \text{(R4)}$$

There is also a small source due to the photolysis of NO_3:

https://doi.org/10.5194/amt-2020-173
Preprint. Discussion started: 23 June 2020


Atmospheric Measurement Techniques Discussions

$$NO_3 + h\nu \rightarrow NO_2 + O, \quad \text{(R5)}$$

but this source is not significant due to the low NO_3 abundance during daytime. NO_2 is converted back into NO through the reaction with oxygen atom (O) in the upper stratosphere (above 40 km):

$$NO_2 + O \rightarrow NO + O_2 \quad \text{(R6)}$$

or via photolysis below 40 km:

$$NO_2 + h\nu \rightarrow NO + O. \quad \text{(R7)}$$

But since NO and NO_2 are quickly interconverted within the NO_x family, Reactions R6 and R7 do not contribute to a net loss of NO_2. The ultimate daytime loss of NO_2 is the reaction with the hydroxyl radicals (OH) that forms HNO_3, which may be transported to the troposphere, followed by rainout:

$$NO_2 + OH + M \rightarrow HNO_3 + M. \quad \text{(R8)}$$

The significant deviation of daytime NO_2 from the model simulation on October 27 was likely due to urban pollution (see section 3.4).

At sunset, the photolytic destruction (Reaction R7) in the upper stratosphere terminates while the conversion of NO (Reaction R2) continues in the lower stratosphere. Meanwhile, the production of O is significantly reduced, which also reduces the loss of NO_2 via Reaction R6. As a result, the total column NO_2 increases by a factor of ~3 at sunset.

Next, the total column NO_2 decreases from $\sim 6.5 \times 10^{15}$ molecules cm^{-2} after sunset to $\sim 4.5 \times 10^{15}$ molecules cm^{-2} before sunrise. During nighttime, NO_2 is converted to N_2O_5 via the reaction with O_3 and NO_3:

$$NO_2 + O_3 \rightarrow NO_3 + O_2, \quad \text{(R9)}$$

$$NO_2 + NO_3 + M \rightarrow N_2O_5 + M. \quad \text{(R10)}$$

Most N_2O_5 stays throughout the night, although there is a small portion that thermally dissociates back to NO_2 and NO_3. Thus, the net effect is a secular decrease in nighttime NO_2.

Finally, at sunrise, photolytic reactions resume, resulting in an abrupt decrease in the total NO_2 column by a factor of ~2 due to Reactions R6 and R7.

https://doi.org/10.5194/amt-2020-173
Preprint. Discussion started: 23 June 2020


Atmospheric Measurement Techniques Discussions

3.2 Vertical profile of NO_2 production and loss

To better understand the contributing factors of the variability of total column NO_2, we show the simulated vertical NO_2 profile in Figure 4. The NO_2 concentration is dominant between 20 km and 40 km (Figure 4a). At noontime, the model NO_2 profile has a peak of $\sim 1.7 \times 10^{15}$ molecules cm^{-2} at 30 km (Figure 4a, orange line). At mid-night, the NO_2 concentration is much higher throughout the stratosphere. The corresponding peak has a larger value of $\sim 2.4 \times 10^{15}$ molecules cm^{-2} and is shifted slightly upward to 32 km (Figure 4a, green line). Therefore, the total column NO_2 is dominated by the variability near 30 km.

The diurnal cycles of the NO_2 concentration at altitudes between 14 km and 38 km are shown in Figure 4b. These cycles show that the daytime increase and the nighttime decrease occur only in the lower stratosphere between 18 km and 34 km. At other altitudes, the daytime and nighttime NO_2 concentrations are relatively constant. The NO_2 cycles closely resemble those of N_2O_5. Figure 5 shows the N_2O_5 concentrations between 14 km and 34 km. During daytime, N_2O_5 is photolyzed into NO_2 and NO_3 through Reaction R4, leading to an increase in the daytime NO_2; during nighttime, NO_2 is thermally converted into N_2O_5 through Reactions R9 and R10, leading to a decrease in the nighttime NO_2. Figure 5 shows that the conversion between the reservoir and NO_2 dominates between 18 km and 34 km, consistent with the NO_2 diurnal cycles. Therefore, the secular NO_2 changes during daytime and nighttime are dominated by N_2O_5 conversions.

3.3 Daytime NO_2 increasing rate

Reactions (R1)–(R5) contribute the daytime increase of NO_2. Sussmann et al. (2005) first obtained a daytime NO_2 increasing rate from ground-based measurements. They reported an annually averaged value of $(1.02 \pm 0.06) \times 10^{14}$ cm^{-2} h^{-1} over Zugspitze, Germany (2.96 km, 47°N). For October alone, they obtained a value of $(1.20 \pm 0.57) \times 10^{14}$ cm^{-2} h^{-1}. For comparison, we calculate the daytime increasing rate using our data between 7 AM and 4 PM. To obtain a rate corresponding to a clean atmosphere, we define a baseline of the diurnal cycle using the 20-percentile in the 15-minute bins from 7 AM to 4 PM (Figure 6). This results in a total of 37 bins, which is roughly the number of points in October shown in Figure 3a of Sussmann et al. (2005). We then apply the linear regression to the baseline and obtain an increasing rate of $(1.29 \pm 0.30) \times 10^{14}$ cm^{-2} h^{-1} in October over TMF (34.4°N). Thus our value is consistent with Sussmann et al.'s (2005) value.

3.4 Temperature sensitivity

The chemical kinetic rates in the model are dependent on temperature. The temperature profile that has been used to obtain the baseline diurnal cycle corresponds to a zonal mean temperature profile at the equinox and 30° latitude (Figure 7, solid line). To test the sensitivity of the simulated 24-hour cycle of NO_2 column, we reduce the input temperature below 60 km by 5 K (Figure 7, dashed line). Note that the 5 K reduction is much larger than the observed tidal variation in stratospheric temperature below 50° latitude, which is ~0.1 K in the lower stratosphere and ~1 K in the middle stratosphere (Sakazaki et al., 2012). We choose this exaggerated reduction in order to clearly show the temperature effect on the NO_2 chemistry.

https://doi.org/10.5194/amt-2020-173
Preprint. Discussion started: 23 June 2020


Atmospheric Measurement Techniques Discussions

Figure 3 (dash-dotted line) shows the simulated NO_2 column using the reduced temperature profile. Because of the reduction in temperature, the nighttime loss due to the reactions with O_3 and NO_3 through Reactions R9 and R10 is slower. As a result, the simulated nighttime NO_2 column is higher than the baseline simulation but it still agrees with the spread of the nighttime observations. In addition, due to the less efficient reaction NO + O_3, the simulated daytime NO_2 column is slightly lower than the baseline simulation but it still agrees with the daytime observation. Thus, given that the tidal temperature change in the middle atmosphere is much smaller than the change in the sensitivity test, the equinox temperature profile used in the baseline run is sufficient for the simulation of the diurnal cycle of the NO_2 column.

3.5 Back-trajectories

Since the TMF is located at the top of a mountain in a remote area, high values of column NO_2 measured on October 27, 2018, were likely due to atmospheric transport of urban pollutants from nearby cities, especially the Los Angeles megacity. While chemical processes would quantitatively alter the amount of NO_2 to be observed over TMF, a back-trajectory study suffices to provide evidence on how the urban pollutants may be transported to TMF.

Figure 8 shows the 24-hour back-trajectories that eventually reached TMF (2.286 km above sea level) at 3 PM during the observational period. These back-trajectories are calculated using the National Oceanic and Atmospheric Administration (NOAA)'s Hybrid Single Particle Lagrangian Integrated Trajectory (HYSPLIT) model (Stein et al., 2015). We use wind fields from the National Centres for Environmental Prediction (NCEP)'s North American Mesoscale (NAM) assimilation at a horizontal resolution of 12 km. To illustrate the wind speed, we plot the 6-hour intervals using the black dots on the trajectories.

The trajectories on 4 of the 6 days (October 23–26) during the observational period converged towards TMF from inland in the north and the east. These inland areas are behind the San Gabriel and San Bernardino Mountain Ranges and are shielded from the urbanized Los Angeles Basin. Therefore, the total column NO_2 measured over TMF on these days closely follow the clean atmosphere simulated by the 1-D model. The trajectories on the other 2 days (October 27–28) converged towards TMF from the Los Angeles Basin in the southwest. But these 2 trajectories were very different. On October 28, the trajectory (Figure 8, purple) came directly from the Pacific Ocean at a relatively high speed, spending only ~4 hours in the Los Angeles Basin before reaching TMF. This fast sea breeze helped reduce the level of accumulated pollutants over the Los Angeles Basin. As a result, the NO_2 level measured at TMF on October 28 was also similar to a clean atmosphere. In contrast, the back-trajectory of October 27 (Figure 8, orange) started going southwestward from the Mojave Desert north of the San Bernardino Mountains at the 24-hour point and passed across the Riverside Basin between the Santa Ana Mountains and San Jacinto Mountains at 18-hour point. The Riverside Basin is one of the most polluted areas in the United States. Then the trajectory continued southwest to pass across the Orange County at the 12-hour point before it turned northwestward towards Downtown Los Angeles at the 6-hour point. Finally, the trajectory turned northeastward and reached TMF. The wind speed over the Los Angeles Basin on October 27 was slower than those in other days, favouring more accumulation of pollutants over the Basin. Thus, the 24-hour back-trajectory on October 27 transported the pollutants in the Riverside Basin and the Los Angeles Basin, resulting a significant surplus of NO_2 in the TMF observation as seen in Figure 3.

https://doi.org/10.5194/amt-2020-173
Preprint. Discussion started: 23 June 2020


Atmospheric Measurement Techniques Discussions

4 Summary

We have presented the diurnal measurements of total column NO_2 that has been made over the TMF located in Wrightwood, California (2.286 km, 34.38°N, 117.68°W) from October 23 to October 28, 2018. The instrument measures the differential slant column NO_2 relative a reference spectrum at the noontime. To retrieve total column NO_2 in the reference spectrum, we applied a variant of the Langley extrapolation. The conventional Langley extrapolation assumes a constant column throughout the day, which does not hold for NO_2. To properly consider the time-dependency of column NO_2, we combine two methods independently developed by Lee et al. (1994) and Herman et al. (2009). The combined method, called the model-based minimum-amount Langley extrapolation, first obtains a baseline of the observed diurnal cycle, which is assumed to be the diurnal cycle in a clean atmosphere. Then the baseline is fitted against the modelled diurnal cycle in a 1-D photochemical model so that the column NO_2 in the reference spectrum is given by the *y*-intercept of the fitted line.

The measured 24-hour cycle of the TMF total column NO_2 on clean days agrees well with a 1-D photochemical model calculation. Our model simulation suggests that the observed monotonic increase of daytime NO_2 column is primarily due to the photodissociation of N_2O_5 in the reservoir. From our measurements, we obtained a daytime NO_2 increasing rate of $(1.29 \pm 0.30) \times 10^{14}$ cm^{-2} h^{-1}, which is consistent with the value observed by Sussmann et al. (2005), who reported a daytime NO_2 increasing rate of $(1.20 \pm 0.57) \times 10^{14}$ over Zugspitze, Germany (2.96 km, 47°N). Our model also suggests that during nighttime, the monotonic decrease of NO_2 is primarily due to the production of N_2O_5. Furthermore, the abrupt NO_2 decrease and increase at sunrise and subset, respectively, are due to the activation and deactivation of the NO_2 photodissociation.

The total column NO_2 in the afternoon on October 27, 2018 was much higher than the model simulation. We conducted a 24-hour HYSPLIT back-trajectory analysis to study how urban pollutants were transported from the Los Angeles Basin. The back-trajectories in 4 of the 6 days during the measurement period went directly from inland desert areas to the TMF. The back-trajectory in another day came from the southwest coastline, spending less than 6 hours over the Los Angeles Basin before reaching the TMF. Lastly, the 24-hour back-trajectory on October 27, 2018 was characterized by a unique slow wind that came from inland in the northeast and spent more than 18 hours in the Los Angeles Basin, picking up pollutants from Riverside, Orange County, and finally Downtown Los Angeles before reaching TMF.

Acknowledgements. The assistance of George Mount (Washington State University) in Langley analysis is greatly appreciated. KFL thanks Sally Newman and Tracy Xia (Bay Area Air Quality Management District) for their assistance in setting up and executing the HYSPLIT model. RK was an undergraduate research assistant under the supervision of KFL. We thank Ralf Sussmann for handling our manuscript and providing useful comments.

Financial support. Support from the NASA SAGE-III/ISS Validation, Upper Atmosphere Research and Tropospheric Composition Programs is gratefully acknowledged. YLY was supported in part by NASA grant P1847132 via UCLA. RK

https://doi.org/10.5194/amt-2020-173
Preprint. Discussion started: 23 June 2020

thanks the generous supports from the AGU Student Travel Grant Award and the Marsh Environmental Sciences Travel Award by the University of California, Riverside.

Data availability. The differential slant column NO_2 used in this paper can be obtained from the supplement of this article.

Supplement. The supplement related to this article is available online.

Author contributions. KFL and TJP prepared the manuscript, with significant conceptual input from SPS and YLY, and critical feedback from all the co-authors. SPS and TJP designed and operated the instrument at the Table Mountain. TJP retrieved the slant column NO_2 from the spectra and developed the Langley method. KFL and YLY performed the model simulations. RK analysed some of the observational and model data.

Competing interests. The authors declare that they have no conflict of interest.

References

Allen, M., Yung, Y. L., and Waters, J. W.: Vertical transport and photochemistry in the terrestrial mesosphere and lower thermosphere (50–120 km), J. Geophys. Res., 86, 3617–3627, https://doi.org/10.1029/JA086iA05p03617, 1981.

Allen, M., Lunine, J. I., and Yung, Y. L.: The vertical-distribution of ozone in the mesosphere and lower thermosphere, J. Geophys. Res., 89, 4841–4872, https://doi.org/10.1029/JD089iD03p04841, 1984.

Ångström, A.: Apparent solar constant variations and their relation to the variability of atmospheric transmission, Tellus, 22, 205–218, https://doi.org/10.3402/tellusa.v22i2.10215, 1970.

Barreto, A., Roman, R., Cuevas, E., Berjon, A. J., Almansa, A. F., Toledano, C., Gonzalez, R., Hernandez, Y., Blarel, L., Goloub, P., Guirado, C., and Yela, M.: Assessment of nocturnal aerosol optical depth from lunar photometry at the Izana high mountain observatory, Atmos Meas Tech, 10, 3007–3019, https://doi.org/10.5194/amt-10-3007-2017, 2017.

Bhartia, P. K., Taylor, S., McPeters, R. D., and Wellemeyer, C.: Application of the Langley plot method to the calibration of the solar backscattered ultraviolet instrument on the Nimbus-7 satellite, J. Geophys. Res. Atmos., 100, 2997–3004, https://doi.org/10.1029/94JD03072, 1995.

Burkholder, J. B., Sander, S. P., Abbatt, J., Barker, J. R., Huie, R. E., Kolb, C. E., Kurylo, M. J., Orkin, V. L., Wilmouth, D. M., and Wine, P. H.: Chemical Kinetics and Photochemical Data for Use in Atmospheric Studies, Evaluation No. 18, JPL Publication 15-10, Jet Propulsion Laboratory, Pasadena, 2015.

Cachorro, V. E., Toledano, C., Berjón, A., de Frutos, A. M., and Sorribas, M.: Comment on "On Langley plots in the presence of a systematic diurnal aerosol cycle centered at noon: A comment on recently proposed methodologies" by F. Marenco, J. Geophys. Res. Atmos., 113, D11210, https://doi.org/10.1029/2007JD009137, 2008.

https://doi.org/10.5194/amt-2020-173
Preprint. Discussion started: 23 June 2020

Camy-Peyret, C.: Balloon-borne infrared Fourier Transform spectroscopy for measurements of atmospheric trace species, Spectrochim. Acta A, 51, 1143–1152, https://doi.org/10.1016/0584-8539(94)00145-2, 1995.

Chen, C. M., Cageao, R. P., Lawrence, L., Stutz, J., Salawitch, R. J., Jourdain, L., Li, Q., and Sander, S. P.: Diurnal variation of midlatitudinal NO_3 column abundance over table mountain facility, California, Atmos. Chem. Phys., 11, 963–978, https://doi.org/10.5194/acp-11-963-2011, 2011.

Crutzen, P. J.: The influence of nitrogen oxides on atmospheric ozone content, Q. J. R. Meteorol. Soc., 96, 320–325, https://doi.org/10.1002/qj.49709640815, 1970.

Fiedler, M., Frank, H., Gomer, T., Hausmann, M., Pfeilsticker, K., and Platt, U.: Ground-based spectroscopic measurements of stratospheric NO_2 and OClO in Arctic winter 1989/90, Geophys. Res. Lett., 20, 963–966, https://doi.org/10.1029/92GL00088, 1993.

Flaud, J. M., Camypeyret, C., Brault, J. W., Rinsland, C. P., and Cariolle, D.: Nighttime and daytime variation of atmospheric NO_2 from ground-based infrared measurements, Geophys. Res. Lett., 15, 261–264, https://doi.org/10.1029/GL015i003p00261, 1988.

Folkner, W. M., Williams, J. G., Boggs, D. H., Park, R. S., and Kuchynka, P.: The Planetary and Lunar Ephemerides DE430 and DE431, JPL Interplanetary Network Progress Report, accessible at http://ipnpr.jpl.nasa.gov/progress_report/42-196/196C.pdf, 42-196, 2014.

Herman, J., Cede, A., Spinei, E., Mount, G., Tzortziou, M., and Abuhassan, N.: NO_2 column amounts from ground-based Pandora and MFDOAS spectrometers using the direct-sun DOAS technique: Intercomparisons and application to OMI validation, J. Geophys. Res. Atmos., 114, D13307, https://doi.org/10.1029/2009JD011848, 2009.

Hönninger, G., von Friedeburg, C., and Platt, U.: Multi axis differential optical absorption spectroscopy (MAX-DOAS), Atmos. Chem. Phys., 4, 231–254, https://doi.org/10.5194/acp-4-231-2004, 2004.

Huber, M., Blumthaler, M., Ambach, W., and Staehelin, J.: Total atmospheric ozone determined from spectral measurements of direct solar UV irradiance, Geophys. Res. Lett., 22, 53–56, https://doi.org/10.1029/94GL02836, 1995.

Iwagami, N., Inomata, S., Murata, I., and Ogawa, T.: Doppler detection of hydroxyl column abundance in the middle atmosphere, J. Atmos. Chem., 20, 1–15, https://doi.org/10.1007/BF01099915, 1995.

Jeong, U., Tsay, S. C., Pantina, P., Butler, J. J., Loftus, A. M., Abuhassan, N., Herman, J. R., Dimov, A., Holben, B. N., and Swap, R. J.: Langley Calibration Analysis of Solar Spectroradiometric Measurements: Spectral Aerosol Optical Thickness Retrievals, J. Geophys. Res. Atmos., 123, 4221–4238, https://doi.org/10.1002/2017JD028262, 2018.

Johnston, P. V., and McKenzie, R. L.: NO_2 observations at 45°S during the decreasing phase of Solar Cycle 21, from 1980 to 1987, J. Geophys. Res. Atmos., 94, 3473–3486, https://doi.org/10.1029/JD094iD03p03473, 1989.

Johnston, P. V., McKenzie, R. L., Keys, J. G., and Matthews, W. A.: Observations of depleted stratospheric NO_2 following the Pinatubo volcanic eruption, Geophys. Res. Lett., 19, 211–213, https://doi.org/10.1029/92GL00043, 1992.

Keys, J. G., and Johnston, P. V.: Stratospheric NO_2 and O_3 in Antarctica: Dynamic and chemically controlled variations, Geophys. Res. Lett., 13, 1260–1263, https://doi.org/10.1029/GL013i012p01260, 1986.

https://doi.org/10.5194/amt-2020-173
Preprint. Discussion started: 23 June 2020

Kreuter, A., Wuttke, S., and Blumthaler, M.: Improving Langley calibrations by reducing diurnal variations of aerosol Ångström parameters, Atmos. Meas. Tech., 6, 99–103, https://doi.org/10.5194/amt-6-99-2013, 2013.

Langley, S. P.: The "solar constant" and related problems, Astrophys. J., 17, 89–99, 10.1086/140999, 1903.

Lee, A. M., Roscoe, H. K., Oldham, D. J., Squires, J. A. C., Sarkissian, A., Pommereau, J. P., and Gardiner, B. G.: Improvements to the accuracy of measurements of NO_2 by zenith-sky visible spectrometers, J. Quant. Spectrosc. Radiat. Transfer, 52, 649–657, https://doi.org/10.1016/0022-4073(94)90031-0, 1994.

Long, C. N., and Ackerman, T. P.: Identification of clear skies from broadband pyranometer measurements and calculation of downwelling shortwave cloud effects, J. Geophys. Res. Atmos., 105, 15609–15626, https://doi.org/10.1029/2000JD900077, 2000.

Marenco, F.: On Langley plots in the presence of a systematic diurnal aerosol cycle centered at noon: A comment on recently proposed methodologies, J. Geophys. Res. Atmos., 112, D06205, https://doi.org/10.1029/2006JD007248, 2007.

May, R. D., and Webster, C. R.: Balloon-borne laser spectrometer measurements of NO_2 with gas-absorption sensitivities below 10-5, Appl. Optics, 29, 5042–5045, https://doi.org/10.1364/AO.29.005042, 1990.

Moreau, G., Robert, C., Catoire, V., Chartier, M., Camy-Peyret, C., Huret, N., Pirre, M., Pomathiod, L., and Chalumeau, G.: SPIRALE: a multispecies in situ balloonborne instrument with six tunable diode laser spectrometers, Appl. Optics, 44, 5972–5989, https://doi.org/10.1364/AO.44.005972, 2005.

Newcomb, S.: Tables of the Sun, Astron. Pap. Amer. Ephem. VI, Part I, 7−170, 1898.

Nizkorodov, S. A., Sander, S. P., and Brown, L. R.: Temperature and pressure dependence of high-resolution air-broadened absorption cross sections of NO_2 (415–525 nm), J. Phys. Chem. A, 108, 4864–4872, https://doi.org/10.1021/jp049461n, 2004.

Noxon, J. F.: Nitrogen dioxide in stratosphere and troposphere measured by ground-based absorption spectroscopy, Science, 189, 547−549, https://doi.org/10.1126/science.189.4202.547, 1975.

Noxon, J. F., Whipple, E. C., and Hyde, R. S.: Stratospheric NO2. Part I. Observational method and behavior at mid-latitude, J. Geophys. Res. Oceans, 84, 5047–5065, https://doi.org/10.1029/JC084iC08p05047, 1979.

Platt, U., Perner, D., and Patz, H. W.: Simultaneous measurement of atmospheric CH_2O, O_3, and NO_2 by differential optical absorption, J. Geophys. Res. Oceans Atmos., 84, 6329−6335, https://doi.org/10.1029/JC084iC10p06329, 1979.

Sakazaki, T., Fujiwara, M., Zhang, X., Hagan, M. E., and Forbes, J. M.: Diurnal tides from the troposphere to the lower mesosphere as deduced from TIMED/SABER satellite data and six global reanalysis data sets, J. Geophys. Res. Atmos., 117, D13108, https://doi.org/10.1029/2011JD017117, 2012.

Sanders, R. W., Solomon, S., Smith, J. P., Perliski, L., Miller, H. L., Mount, G. H., Keys, J. G., and Schmeltekopf, A. L.: Visible and near-ultraviolet spectroscopy at McMurdo station, Antarctica. Part 9: Observations of OClO from April to October 1991, J. Geophys. Res. Atmos., 98, 7219–7228, https://doi.org/10.1029/93JD00042, 1993.

Shaw, G. E.: Error analysis of multi-wavelength sun photometry, Pure Appl. Geophys., 114, 1–14, https://doi.org/10.1007/BF00875487, 1976.

https://doi.org/10.5194/amt-2020-173
Preprint. Discussion started: 23 June 2020

Solomon, S.: Stratospheric ozone depletion: A review of concepts and history, Rev. Geophys., 37, 275–316, https://doi.org/10.1029/1999RG900008, 1999.

Stein, A. F., Draxler, R. R., Rolph, G. D., Stunder, B. J. B., Cohen, M. D., and Ngan, F.: NOAA's HYSPLIT atmospheric transport and dispersion modeling system, Bull. Amer. Meteorol. Soc., 96, 2059–2077, https://doi.org/10.1175/BAMS-D-14-00110.1, 2015.

Stutz, J., and Platt, U.: Numerical analysis and estimation of the statistical error of differential optical absorption spectroscopy measurements with least-squares methods, Appl. Optics, 35, 6041−6053, https://doi.org/10.1364/AO.35.006041, 1996.

Sussmann, R., Stremme, W., Burrows, J. P., Richter, A., Seiler, W., and Rettinger, M.: Stratospheric and tropospheric NO_2 variability on the diurnal and annual scale: a combined retrieval from ENVISAT/SCIAMACHY and solar FTIR at the Permanent Ground-Truthing Facility Zugspitze/Garmisch, Atmos. Chem. Phys., 5, 2657–2677, https://doi.org/10.5194/acp-5-2657-2005, 2005.

Toledano, C., González, R., Fuertes, D., Cuevas, E., Eck, T. F., Kazadzis, S., Kouremeti, N., Gröbner, J., Goloub, P., Blarel, L., Román, R., Barreto, Á., Berjón, A., Holben, B. N., and Cachorro, V. E.: Assessment of Sun photometer Langley calibration at the high-elevation sites Mauna Loa and Izaña, Atmos. Chem. Phys., 18, 14555−14567, https://doi.org/10.5194/acp-18-14555-2018, 2018.

Wang, S., Pongetti, T. J., Sander, S. P., Spinei, E., Mount, G. H., Cede, A., and Herman, J.: Direct Sun measurements of NO_2 column abundances from Table Mountain, California: Intercomparison of low- and high-resolution spectrometers, J. Geophys. Res. Atmos., 115, D13305, https://doi.org/10.1029/2009JD013503, 2010.

Woolard, E. W.: Theory of the rotation of the Earth around its center of mass, Astron. Pap. Amer. Ephem. XV, Part I, 1−165, 1953.

https://doi.org/10.5194/amt-2020-173
Preprint. Discussion started: 23 June 2020

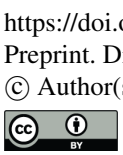

Atmospheric Measurement Techniques Discussions

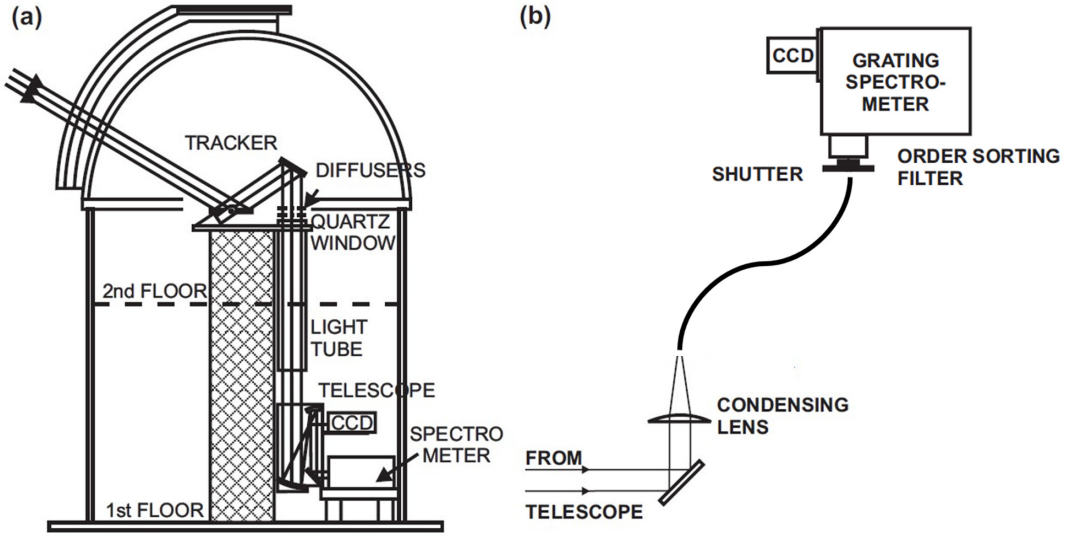

Figure 1: Schematic of the instrument light path over the Table Mountain Facilities (TMF, 2.286 km above mean sea level, 34.38°N, 117.68°W), Wrightwood, California, USA. (a) Light is collected by the primary of the heliostat (tracker), reflected down to the telescope on the first floor which conditions it to a 7-cm diameter beam. (b) The light is then reflected to a condensing lens into a fibre optic bundle, past a shutter, order-sorting filter, and then into the spectrometer. The fibre bundle contains 19 fibres in a round pattern at the entrance, and at the exit fibres are arranged in a line pattern that is set parallel to the spectrometer slit.

https://doi.org/10.5194/amt-2020-173
Preprint. Discussion started: 23 June 2020

Atmospheric Measurement Techniques Discussions

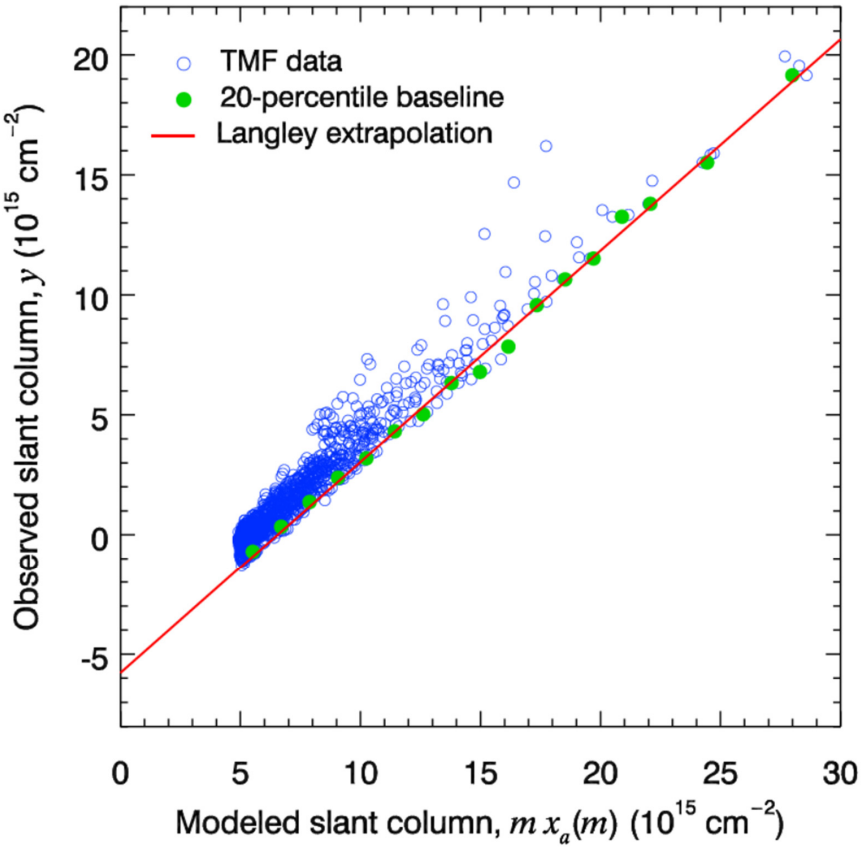

Figure 2. The model-based minimum-amount Langley extrapolation. The blue circles are the observed differential slant columns during our campaign over TMF from October 23 to October 28, 2018. Each observational value is plotted against the total slant column modelled at the same time of the day (e.g. 11:05 AM PST). The green dots are the 20-percentile of 20 uniform bins on the $\boldsymbol{x}$-axis. The red line is a linear regression of the green dots, which is taken as the diurnal cycle in a clean atmosphere. The linear fit is $\boldsymbol{y = 0.88\, m\, x_a(m) - 5.77 \times 10^{15}}$. The $\boldsymbol{y}$-intercept gives the reference column, $\boldsymbol{y_0 = 5.77 \times 10^{15}}$ molecules cm^{-2}.

https://doi.org/10.5194/amt-2020-173
Preprint. Discussion started: 23 June 2020

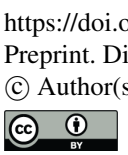

Atmospheric Measurement Techniques Discussions

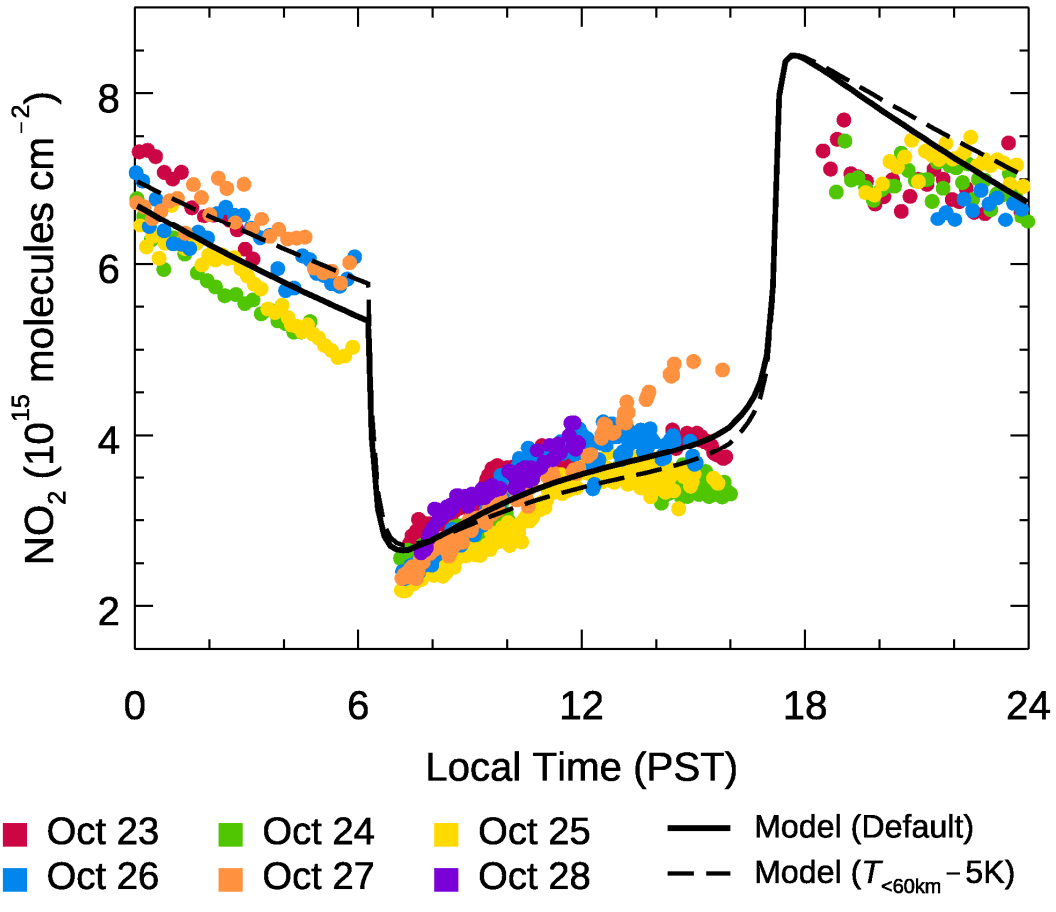

Figure 3: The total column NO_2 abundance measured over TMF on October 23–28, 2018, represented by the color dots. The 1-D model simulation, with default input temperature and surface N_2O being 330 ppb, representing October 26 is shown as the solid black line. An additional 1-D model simulation with temperature below 60 km reduced by 5 K, is shown as the dashed line.

https://doi.org/10.5194/amt-2020-173
Preprint. Discussion started: 23 June 2020

Atmospheric Measurement Techniques Discussions

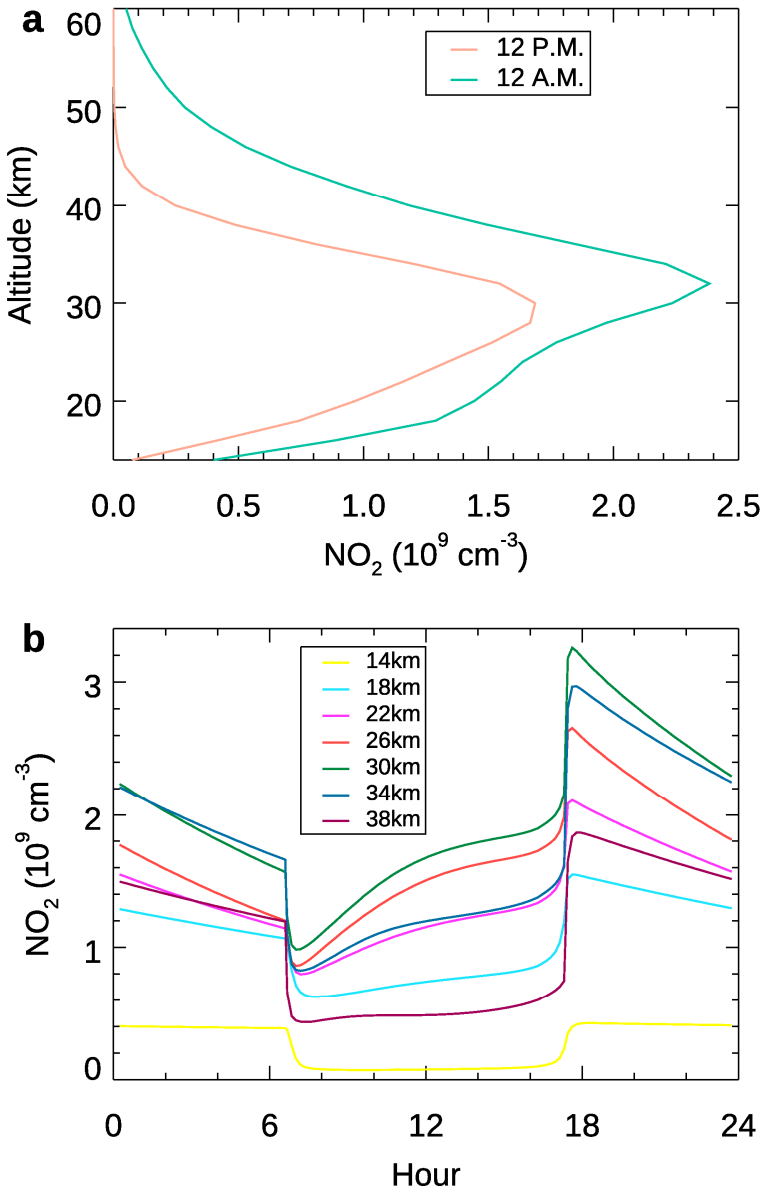

455

Figure 4: Simulated vertical NO_2 concentration. (a) The simulated NO_2 vertical concentration between 14−38 km at 00:00 PST (green) and 12:00 PST (orange) corresponding to October 27 in the 1-D photochemical model. (b) Same as (a) except the simulated NO_2 variation over the 24 hours at selected altitudes.

https://doi.org/10.5194/amt-2020-173
Preprint. Discussion started: 23 June 2020

Atmospheric Measurement Techniques Discussions

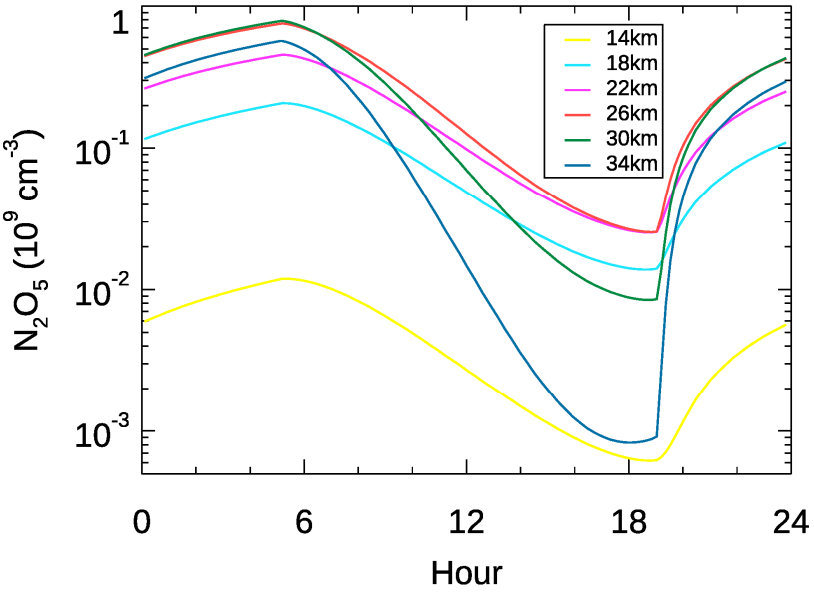

460 **Figure 5. Same as Figure 4(b) except for N_2O_5.**

https://doi.org/10.5194/amt-2020-173
Preprint. Discussion started: 23 June 2020

Atmospheric Measurement Techniques Discussions

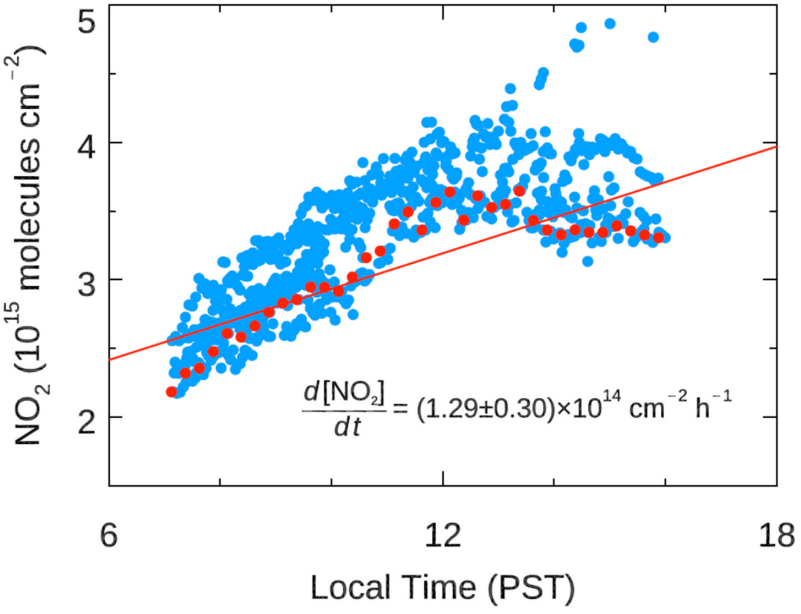

Figure 6. The daytime NO_2 increase obtained from the baseline of the observed diurnal variability. The blue points are the same as the daytime data shown in Figure 3. The red points are the 20-percentile of the daytime data in 15-minute intervals between 7 AM to 4 PM, which form a baseline of the daytime variability. The daytime NO_2 increase rate, obtained from the linear regression of the red points, is $(\mathbf{1.29 \pm 0.30}) \times \mathbf{10^{14}}$ cm^{-2} h^{-1}.

https://doi.org/10.5194/amt-2020-173
Preprint. Discussion started: 23 June 2020

Atmospheric Measurement Techniques Discussions

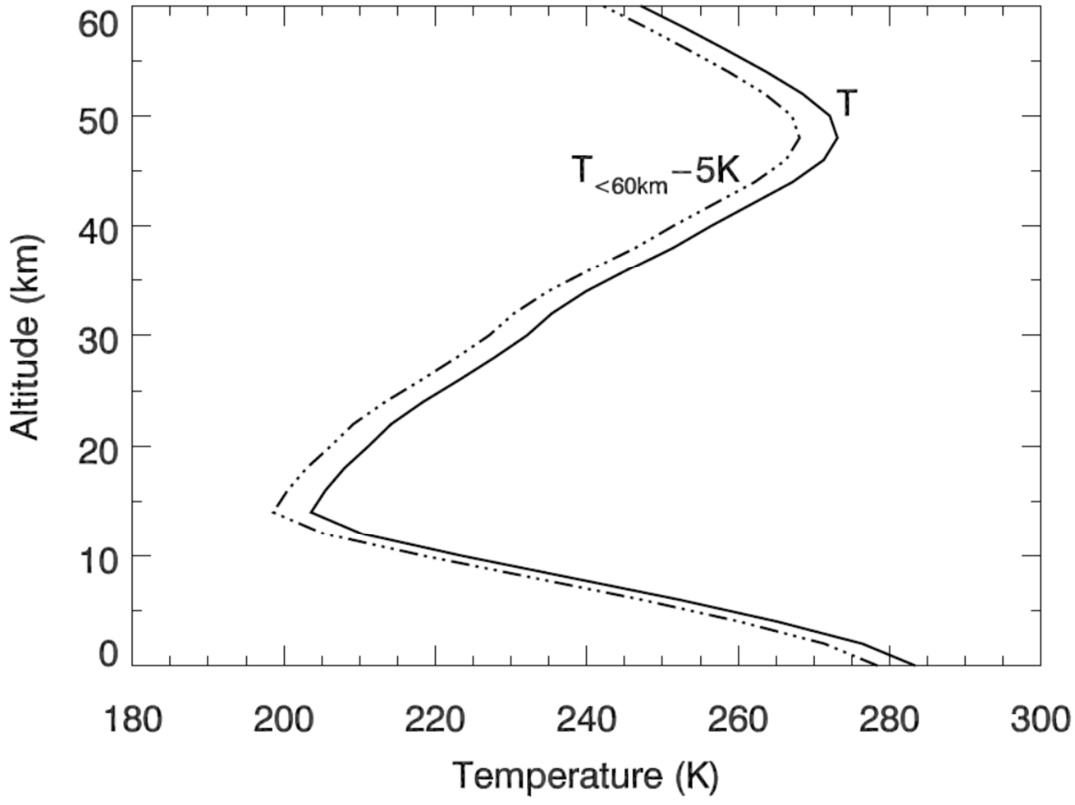

Figure 7: The temperature profiles used in the 1-D Caltech/JPL photochemical model: the baseline profile (solid line) based on the equinox zonal average at 30° latitude and the modified profile where the temperature below 60 km is reduced by 5 K (dash-dotted line).

https://doi.org/10.5194/amt-2020-173
Preprint. Discussion started: 23 June 2020

Atmospheric Measurement Techniques Discussions

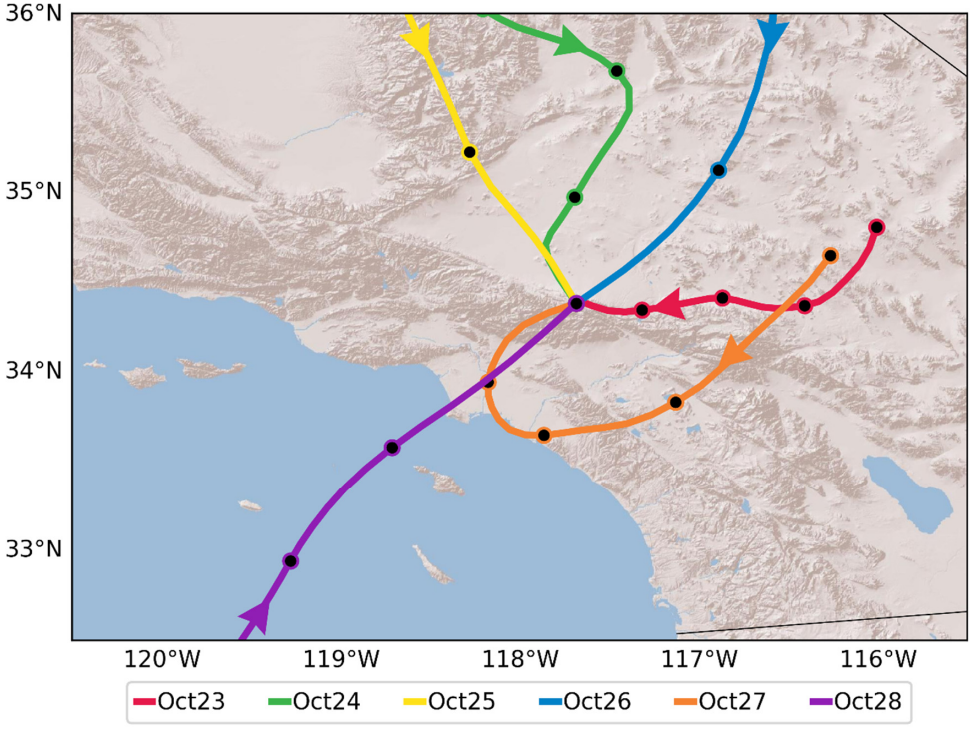

Figure 8: The 24-hour back-trajectories of ambient air flow that reached TMF at 15:00 PST on each day from October 23 to October 28, 2018. The colour codes are the same as those used in Figure 3. The black dots represent the 6-hour intervals on the trajectories.